SAND2019-5682C

Validation of calibrated k-ϵ model parameters for jet-in-crossflow

Nathan E. Miller*, Steven J. Beresh†,
Sandia National Laboratories, Albuquerque, NM, 87185
&
Jaideep Ray‡
Sandia National Laboratories§, Livermore, California 94550

Previous efforts determined a set of calibrated model parameters for Reynolds-Averaged Navier Stokes (RANS) simulations of a compressible jet in crossflow (JIC) using a k-ϵ turbulence model. These coefficients were derived from Particle Image Velocimetry (PIV) data of a complementary experiment using a limited set of flow conditions. Here, k-ϵ models using conventional (nominal) and calibrated parameters are rigorously validated against PIV data acquired under a much wider variety of JIC cases, including a flight configuration. The results from the simulations using the calibrated model parameters showed considerable improvements over those using the nominal values, even for cases that were not used in defining the calibrated parameters. This improvement is demonstrated using quality metrics defined specifically to test the spatial alignment of the jet core as well as the magnitudes of flow variables on the PIV planes. These results suggest that the calibrated parameters have applicability well outside the specific flow case used in defining them and that with the right model parameters, RANS results can be improved significantly over the nominal.

I. Introduction

The jet-in-crossflow (JIC) problem has been studied via a large number of both experimental and numerical studies (e.g., [1, 2]), which have provided considerable understanding of the flow topology and statistics [3, 4]. The flowfield is typified by a counter-rotating vortex pair (CVP) oriented in the streamwise direction in the jet core and a horseshoe vortex (HSV) near the wall which wraps around the jet column. The interaction of the CVP and HSV with downstream control surfaces like fins has been shown to alter the effective forces generated by those surfaces by altering their effective angle of attack [5, 6, 7].

For the purposes of vehicle design, accurate modeling of the complex flow features at downstream control surfaces is a primary goal [8]. Unfortunately, most numerical approaches are so

*Technical Staff, Aerosciences Department, nmille1@sandia.gov
†Technical Staff, Aerosciences Department, AIAA Associate Fellow, sjberes@sandia.gov
‡Technical Staff, Extreme-scale Data Science & Analytics, jairay@sandia.gov

computationally prohibitive that Reynolds-Averaged Navier Stokes (RANS) continues to be the most efficient investigative technique. Arunajatesan [9] tested multiple two-equation RANS models for simulating a supersonic jet in a transonic, compressible crossflow and concluded that most of their predictive capabilities were "marginal at best." Although the RANS results were qualitatively similar to the experimental data used for comparison, inaccuracies in the turbulent stress predictions resulted in the incorrect location and strength of the CVP and an overpredicted velocity deficit in the jet core. These shortcomings will, in turn, lead to poor estimations of the effective forces on downstream control surfaces.

The RANS data used by Arunajatesan [9] were produced using nominal model parameters (C_{nom}). This led Ray *et al.* [10] to investigate the usefulness of rigorously tuning the parameters of the k-ϵ model in hopes of producing the best possible results. Short of making structural changes to the turbulent stress model within RANS, the best results that can be accomplished come by calibrating the model's existing parameters to the specific flow case of interest. Ray *et al.* [10] proposed a Bayesian inverse problem and a Markov chain Monte Carlo method utilizing PIV data of the streamwise vorticity to determine an optimum, calibrated combination of the three model parameters (C_{opt}) for a single case of the jet-in-crossflow problem. Ray *et al.* [11] continued this work by calibrating the parameters for a wider set of flow cases and showed improvement for modeled vorticity in each case. The calibration process that led to the determination of C_{opt} was performed by matching to a single streamwise vorticity core on a y-z flow-normal crossplane. Although the model fit to that variable was much improved under those narrow conditions, little validation of the use of C_{opt} under different flow conditions or on other variables or in other regions of the flow has been done. This work is an effort to take C_{opt} as determined by matching the streamwise vorticity at a single location, then validate its usefulness in improving RANS predictions of multiple flow variables throughout the domain under a variety of flow characteristics.

To that end, a large set of PIV data collected over many years at Sandia National Laboratories (SNL) was tapped to provide the experimental data needed for the validation of RANS simulations (Sect. II). Variables of interest were taken from the converged RANS results and comparisons were made to the PIV data using three quality metrics, each specifically chosen to give a different measure of the quality of the simulation results (Sect. III). Side-by-side comparisons of the RANS results and PIV data, along with the values of the quality metrics for each variable on each plane for each case being investigated, show that the use of C_{opt} produces superior simulation results, even for flow cases that differ considerably from the case used for the parameter calibration (Sect. IV).

II. Experiments and Data

A. PIV

PIV data from two separate experimental campaigns, performed in different wind tunnels with different equipment and geometries, are used here for validation. The first sets of data, against which the nominal and calibrated RANS simulations were tested, were collected in the Trisonic Wind Tunnel (TWT) at SNL and have been reported on and used in a number of previous studies (e.g., [7, 8, 12, 13, 14]). The data are all from jet-in-crossflow experiments each consisting of a wall-mounted nozzle venting a supersonic jet into a subsonic (Mach 0.8) crossflow (Figure 1). The TWT cross section is 305×305 mm and the tunnel was operated with a freestream velocity of 285±2 m/s. Four different jet nozzles were used for separate tests, each with a design Mach number of 3.7 at the centerline of the nozzle exit. The first was oriented normal to the tunnel floor

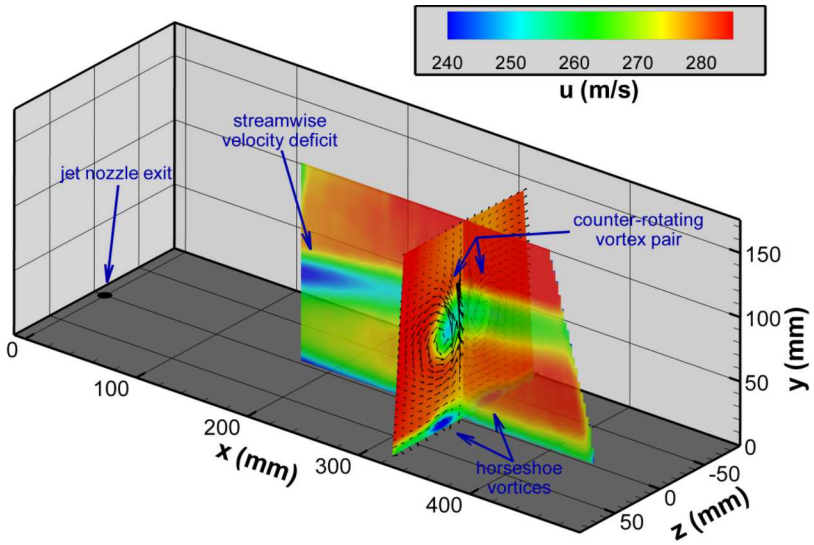

Figure 1: Schematic of the TWT and mean JIC flow topology depicted using PIV data from Beresh *et al.* [12] and Beresh *et al.* [13] and collected on the x-y centerplane and a y-z crossplane at $x = 321.8$ mm. Figure previously used in Ray *et al.* [10] and used with permission.

and thus vented the jet perpendicularly into the subsonic crossflow. The additional nozzles were inclined laterally to the freestream direction at angles of $\alpha = 15°$, 30°, and 45° and thus vented the jet into the crossflow perpendicularly to the freestream but canted in the crossplane. The nozzle with $\alpha = 0°$ had an exit diameter of 9.53 mm while the remaining nozzles had elliptical exits resulting from the design which was based on a conical nozzle being scarfed by the plane of the tunnel wall passing through the centerpoint of the exit plane of the normal conical nozzle. Further dimensions and nozzle exit properties can be found in Beresh *et al.* [14].

PIV datasets were collected during multiple experiments in the TWT with nozzles of each of the inclination angles and at five different jet-to-freestream dynamic pressure ratios (J). Across the different experiments, data were collected on three different two-dimensional (2D) planes within the tunnel. The first plane was the x-y centerplane which was aligned with the nozzle center ($z = 0$) and extended from ≈ 226 to 350 mm downstream of the nozzle. Data were collected on the centerplane only with the $\alpha = 0°$ nozzle and only for $J = 8.1$ and $J = 10.2$ [15]. The second plane was a y-z crossplane positioned at $x = 219$ mm (23.0 jet diameters) and roughly centered around $z = 0$. Data were collected on this crossplane during experiments with both the $\alpha = 0°$ and $\alpha = 30°$ jet nozzles, both with $J = 10.2$ [7]. The final plane was also a y-z crossplane, but was positioned at $x = 321.8$ mm (33.8 jet diameters). It was at this downstream location that the data used in Ray *et al.* [10] were taken. The data they used were taken with the 0°-inclined nozzle operating at a dynamic pressure ratio of $J = 10.2$ and had been previously reported in Beresh *et al.* [13]. Herein, data that were collected on this crossplane for experiments using all four nozzles at J values of 2.8, 5.6, 8.1, 10.2, and 16.7 are used (Table 1). This is a combination of the datasets reported in Beresh *et al.* [13] and Beresh *et al.* [14].

The PIV data taken in the TWT were all collected using conventional stereoscopic procedures with cameras positioned on Scheimpflug mounts. For both the centerplane and the upstream crossplane, the two cameras (LaVision sCMOS, 5.5MP) were fitted with 200 mm lenses and data were collected at 10 Hz. For the centerplane, the two cameras were mounted on the same side of the tun-

Table 1: The planes of PIV data used for each combination of nozzle inclinations (α) and dynamic pressure ratios (J).

	J = 2.8	J = 5.6	J = 8.1	J = 10.1	J = 16.7
α = 0°	x = 321.8 mm	x = 321.8 mm	z = 0.0 mm x = 321.8 mm	z = 0.0 mm x = 219 mm x = 321.8 mm	x = 321.8 mm
α = 15°	x = 321.8 mm	x = 321.8 mm	x = 321.8 mm	x = 321.8 mm	x = 321.8 mm
α = 30°	x = 321.8 mm	x = 321.8 mm	x = 321.8 mm	x = 219 mm x = 321.8 mm	x = 321.8 mm
α = 45°	x = 321.8 mm	x = 321.8 mm	x = 321.8 mm	x = 321.8 mm	x = 321.8 mm

nel at a half-angle of 20°, while geometric restrictions with the positioning of windows in the TWT required that the cameras be mounted downstream of the plane with one camera on either side of the tunnel for the upstream crossplane. This resulted in a camera half-angle of 55° in the horizontal plane with each camera pointed at a slight upward angle of 15°. For the downstream crossplane, the cameras (Redlake MegaPlus ES4.0/E) were fitted with 105 mm lenses (Nikon Micro-Nikkor) and were both mounted on the same side of the tunnel. As depicted in Beresh *et al.* [13], the cameras viewed the laser sheet from opposite directions with the help of mirrors rigidly mounted inside the plenum. This resulted in an effective camera half-angle of 53°. The data were collected for this plane at 5 Hz.

Light for the PIV system in the TWT was produced by a frequency-doubled dual-cavity Nd:YAG laser (Spectra Physics PIV-400) at 300-400 mJ per beam for both the centerplane and the upstream crossplane data collection. It was focused to a thickness of 1.5 mm for the centerplane and about 2 mm for the crossplane. For the downstream crossplane, a pair of frequency-doubled Nd:YAG lasers (Coherent Infinity 40-100) which produced about 120 mJ per beam were used and were focused to a laser-sheet thickness of 2.0 mm.

The second set of data, collected during a different experimental campaign, was previously reported in Beresh *et al.* [8]. Those data were collected during experiments performed on a full-scale flight vehicle model in a production-scale wind tunnel under a variety of conditions and represent the most complex and flight-realistic data against which the calibrated RANS could be tested. The experiments were performed in the NASA Ames Unitary Plan Wind Tunnel which, with its 3.4×3.4 m cross section, was able to hold a 3.6 m long, full-scale reproduction of an axisymmetric flight vehicle with four aft fins. Two nozzles were mounted into the model surface at approximately the model's midsection and had a lateral inclination angle of 39.5° to the surface normal. The nozzles were considerably larger than those used in the TWT, with an effective nozzle diameter at the model surface plane of 38.2 mm. The nozzles were designed to produce a nominal Mach number at the centerline of the nozzle exit of 3.66 by utilizing high-pressure room-temperature air which was supplied at up to 20 MPa at 18 kg/s through the mounting sting. A variety of tests were performed during the experimental campaign, as explained in Beresh *et al.* [8], with different freestream Mach numbers, dynamic pressure ratios, and angles of attack. Only the baseline case from that campaign is used here. That case used a jet stagnation pressure of 2.83 MPa while the wind tunnel was operated at a freestream Mach number of 0.8 with a stagnation pressure of 33.5

kPa, resulting in a jet-to-freestream dynamic pressure ratio of $J = 16$.

PIV data were collected on a set of y-z planes at a range of x locations from 414 to 820 mm downstream of the nozzle center. The cameras (Redlake MegaPlus ES4.0), with their 85 mm lenses, were mounted on Scheimpflug mounts in the plenum on one side of the tunnel such that they viewed the laser sheet from opposite sides. Four Nd:YAG lasers (New Wave Gemini 120) were used, with two sets of two each working in tandem for the initial and delayed pulses. Beams were directed into the tunnel on the opposite side from the cameras via mirrors mounted into the tunnel plenum. Laser sheet thicknesses were 1.5 mm and 3.0 mm for the initial and delayed pulses respectively. The reflecting mirror and the cameras were mounted on a traverse system that allowed for PIV planes to be collected throughout the range of x locations. Herein, data from only the $x = 820$ mm plane were used for comparisons to the RANS simulation data, though future work may include comparisons to data taken throughout the range of the traverse.

B. RANS

The RANS data, produced with both C_{nom} and C_{opt}, were generated using Sandia National Laboratories' parallel compressible gas dynamics code, SIERRA/Aero. The specifics of the k-ϵ model that is utilized in SIERRA/Aero are described in So *et al.* [16] and Brinkman *et al.* [17]. The model uses three parameters, $\{C_\mu, C_{\epsilon 1}, C_{\epsilon 2}\}$. C_{nom} was defined as $\{0.9, 1.43, 1.92\}$ for the model parameters, respectively, (see Brinkman *et al.* [17]) while C_{opt} was defined as $\{0.1025, 1.416, 2.099\}$ as specified in Ray *et al.* [10].

For the experiments performed in the TWT, a multiblock structured mesh of ≈ 3.14 million grid cells was defined from ≈ 32.0 jet diameters upstream to ≈ 100 jet diameters downstream of the jet nozzle. The spanwise and wall-normal dimensions were defined to match those of the TWT and the nozzle geometry was resolved down to the stagnation chamber. A previous grid refinement study on a limited subset of the cases studied here demonstrated that this resolution was approximately at the threshold of the minimum required to eliminate numerical errors. It may be possible, especially for the cases studied here but not used in the resolution study, that some minor differences would be found with a higher resolution grid. Investigation of the impact of this is ongoing. Simulations were run using each of the parameter sets for each of the needed combinations of the nozzle inclination angles and dynamic pressure ratios. After reaching convergence, data for all pertinent variables were extracted from each simulation on the same planes upon which the PIV data were collected.

For simulating the experiment performed on the flight vehicle model, a multiblock structured mesh of ≈ 25.7 million hex elements was defined that included the entire flight vehicle but with far field boundaries instead of defining the NASA Ames tunnel. The flight vehicle, including the tail fins, was resolved within the mesh along with the two nozzles mounted into the model surface as defined in Beresh *et al.* [8]. Internal convergence studies have shown that this mesh results in converged integrated forces and moments though some residual convergence may still be possible in the far-off-body flow. Again the appropriate planes of data were extracted from the results of simulations run with each set of model parameters so that direct comparisons could be made to the PIV data.

III. Methods

In order to quantitatively assess the quality of the improvement to the RANS results by switching from C_{nom} to C_{opt} three metrics were used to measure the spatial and magnitude differences

between the PIV and RANS datasets. Similar metrics have been proposed for use in environmental fluid dynamics studies for evaluating the accuracy of plume models [18] and have been used by others for comparing models to large experimental datasets (e.g., [19, 20]). These three metrics each measure the accuracy of the modeled data in different ways and provide a more rigorous comparison than tracking only a singular peak value or peak alignment.

The first metric was the mean squared error normalized by the mean squared magnitude of the PIV data. This is defined as,

$$MSE = \frac{\langle (X_{PIV,i,j} - X_{RANS,i,j})^2 \rangle}{\left\langle X_{PIV,i,j}^2 \right\rangle}, \tag{1}$$

where X_{PIV} and X_{RANS} represent any given dependent variable from the PIV and RANS, respectively, the $\langle\rangle$ represent an average taken over the 2D plane being tested, and MSE goes to zero for a perfect model fit. The normalization of the mean squared error was done in order to allow for direct comparisons of MSE across different flow variables which had differing mean orders of magnitude. For example, if a traditional mean squared error were to be used, values for errors on velocity values would be orders of magnitude different than errors on the vorticity, making comparisons difficult. The mean squared error has been used extensively as a quality metric but has the flaw that it is susceptible to biases created by extreme events or outliers in experimental data, especially when those data cross multiple orders of magnitude [18]. Specifically, a few outlying points of large magnitude that produce even relatively small errors can bias the MSE regardless of the quality of the fit over the remaining data in the domain. Small relative errors at large magnitude points swamp all the large relative errors at lower magnitude points.

In an effort to reduce this bias and quantify improvements while minimizing the effects of outliers, the second metric used was the geometric mean of the errors normalized by the geometric mean of the magnitudes defined as,

$$GME = \frac{\exp\left[\langle \ln(|X_{PIV,i,j} - X_{RANS,i,j}|) \rangle\right]}{\exp\left[\langle \ln(|X_{PIV,i,j}|) \rangle\right]}. \tag{2}$$

By not using squares and by taking the mean of the model-to-experiment difference in logarithmic space, this metric reduces the bias toward errors at high magnitude points. In that way, the GME does a better job than the MSE when data cover multiple orders of magnitude; it minimizes the bias of smaller errors in large numbers swamping larger errors in smaller numbers[a]. GME can therefore be seen as a measure of how well the RANS does at predicting values away from the most extreme-valued regions of the flow while MSE is a measure of how well the RANS predicts those peak values.

The final metric was the 2D correlation coefficient defined as,

$$corr = \frac{\sum_j \sum_i \left[(X_{PIV,i,j} - \langle X_{PIV} \rangle)(X_{RANS,i,j} - \langle X_{RANS} \rangle) \right]}{\sqrt{\sum_j \sum_i \left[(X_{PIV,i,j} - \langle X_{PIV} \rangle)^2 \right] \sum_j \sum_i \left[(X_{RANS,i,j} - \langle X_{RANS} \rangle)^2 \right]}}. \tag{3}$$

The 2D correlation can take values between -1.0 and 1.0 and represents a measure of the spatial alignment between the two datasets. The magnitudes of the RANS-predicted values are of no consequence to $corr$ and an ideal value of 1.0 is still possible if the RANS values are wrong everywhere but are high when the PIV values are high and are low when the PIV values are low. If $corr = 0$ it suggests that the RANS results are no better than a random number distribution.

[a]This definition of GME should not be confused with the "geometric mean bias" defined in Chang and Hanna [18], which is undefined for a dependent variable with negative values and which has problems with positive values less than unity.

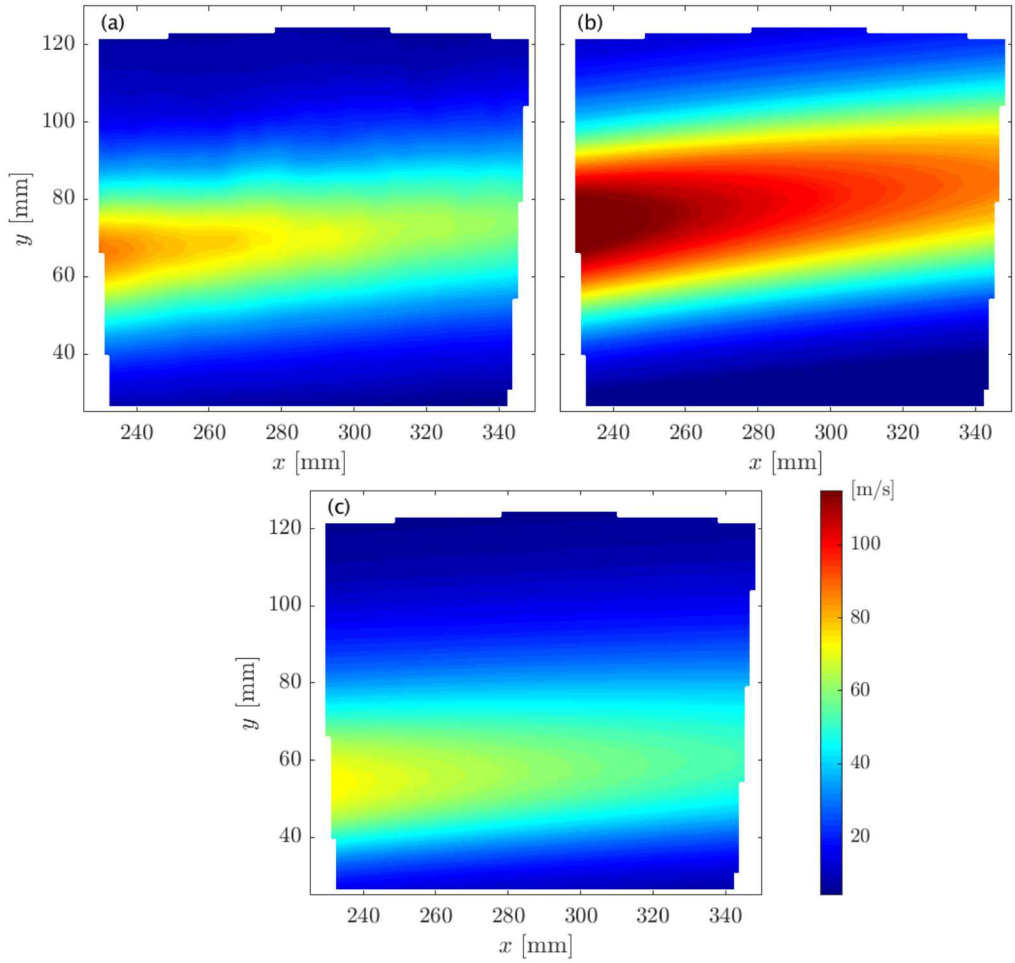

Figure 2: The wall-normal velocity (V_y) on the centerplane for the uncanted nozzle (α = 0°) with J = 10.2 as collected from the PIV experiment (a), as determined by RANS using C_{nom} (b), and using C_{opt} (c).

IV. Results

Given that a total of 40 different RANS simulations were run for this work, and a total of 48 independent planes of data were taken to use for comparison to the PIV, it is infeasible to show contour plots of even one variable from every plane. We therefore chose only four sets of contour plots to demonstrate the general impact that the use of C_{opt} had compared to C_{nom} and also restrict ourselves to only two flow variables for comparisons across all planes.

First, the wall-normal velocity (V_y) has been used as an indicator of the location, strength, and spacing of the counter-rotating vortex pair (CVP) that typifies the JIC interaction [12]. As such, it was decided that V_y should be a primary variable used for quantifying the accuracy of the RANS simulations, especially on the centerplane. For the case where α = 0° and J = 10.2, the RANS simulation performed with C_{nom} significantly overestimated V_y on the centerplane, which also led to the centerline of the jet core being farther from the wall and increasing its distance from the wall at a faster rate with downwind distance than was observed in the PIV (Figure 2). Conversely, when C_{opt} was used, the magnitude of V_y was considerably reduced, but was overcorrected somewhat resulting in the jet core being closer to the tunnel wall than was observed in the PIV.

Table 2: Quality metrics for V_y on the centerplane as depicted in Figure 2.

	$corr$	MSE [m^2/s^2]	GME [m/s]
C_{nom}	0.802	0.506	0.575
C_{opt}	0.789	0.119	0.306

Because the RANS results predicted by using C_{nom} were better aligned with the PIV results at the upstream edge of the domain and because the extents of the modeled jet were so much larger, thus overlapping the PIV data, that simulation achieved a slightly higher $corr$ than did the results predicted with C_{opt}. The modeled jet based on C_{opt} had the jet centerline too close to the wall. However, because the magnitudes of V_y were consistently overpredicted throughout the core in the C_{nom} simulation, the MSE and GME values for that data were worse than those determined for the C_{opt}-derived results (Table 2).

The magnitude of the V_y values is often an indicator of the strength of the circulation in the CVP that is drawing fluid up through the middle of the jet core. The higher V_y magnitudes observed when C_{nom} was used suggested that the CVP had a stronger vorticity magnitude and/or that the lateral separation between the counter-rotating cores was different than what was expected based on the PIV or what was seen when C_{opt} was used. This can be seen on the crossplanes by looking at the streamwise vorticity ($\overline{\omega} = (d\overline{V_z}/dy - d\overline{V_y}/dz)/2$), which was the variable used by Ray *et al.* [10] in obtaining C_{opt}, and which was chosen here as the second variable for quantifying the accuracy of the RANS results.

For the case where $\alpha = 0°$, $J = 10.2$, and on the plane where $x = 219$ mm, the RANS results from using C_{nom} do indeed show CVP core vorticities that are stronger than were observed in the PIV and that the cores are farther from the wall and closer together (Figure 3). This is consistent with the nominal results shown in both Arunajatesan [9] and Ray *et al.* [10]. The use of C_{opt} resulted in a lowering of the location and of the strength of the vorticity in the CVP cores, but as with V_y, the correction may have been by too much as the cores moved closer to the wall than was seen in the PIV. This again led to the C_{nom}-derived data having a better $corr$ value than did the C_{opt}-derived data (Table 3). The correction in the strength of the vorticity in the CVP cores by using C_{opt} did result in a reduction in MSE, but the value of GME was actually slightly worsened. This suggests that although the most extreme vorticity values in the CVP cores were more accurate while using C_{opt}, moderate vorticity values elsewhere in the crossplane may have been made slightly worse, a result that may also be tied to the issue with the spatial alignment.

This is also particularly interesting because Ray *et al.* [10] used this exact variable from this exact case for determining C_{opt}, but the data used there were from the plane at $x = 321.8$ mm. When the quality metrics for that plane are investigated, all three did indeed improve with C_{opt}. This may suggest that in correcting the location and magnitude of the vorticity at $x = 321.8$ mm, the calibration overcorrected the location and intensity at $x = 219$ mm. This would in turn suggest that there is some other issue causing the trajectory of the jet core to be incorrect, such that it overshoots the right location at $x = 321.8$ mm when it is correct at 219 mm or undershoots the correct location at $x = 219$ mm when correct at 321.8 mm. Surprisingly, this is the worst result that was seen among all of the sets of quality metrics calculated (can be seen as the black circles on the wrong side of the lines in Figures 6(b) and (c) later).

A much more noticeable improvement in the RANS results based on C_{opt} was seen for the

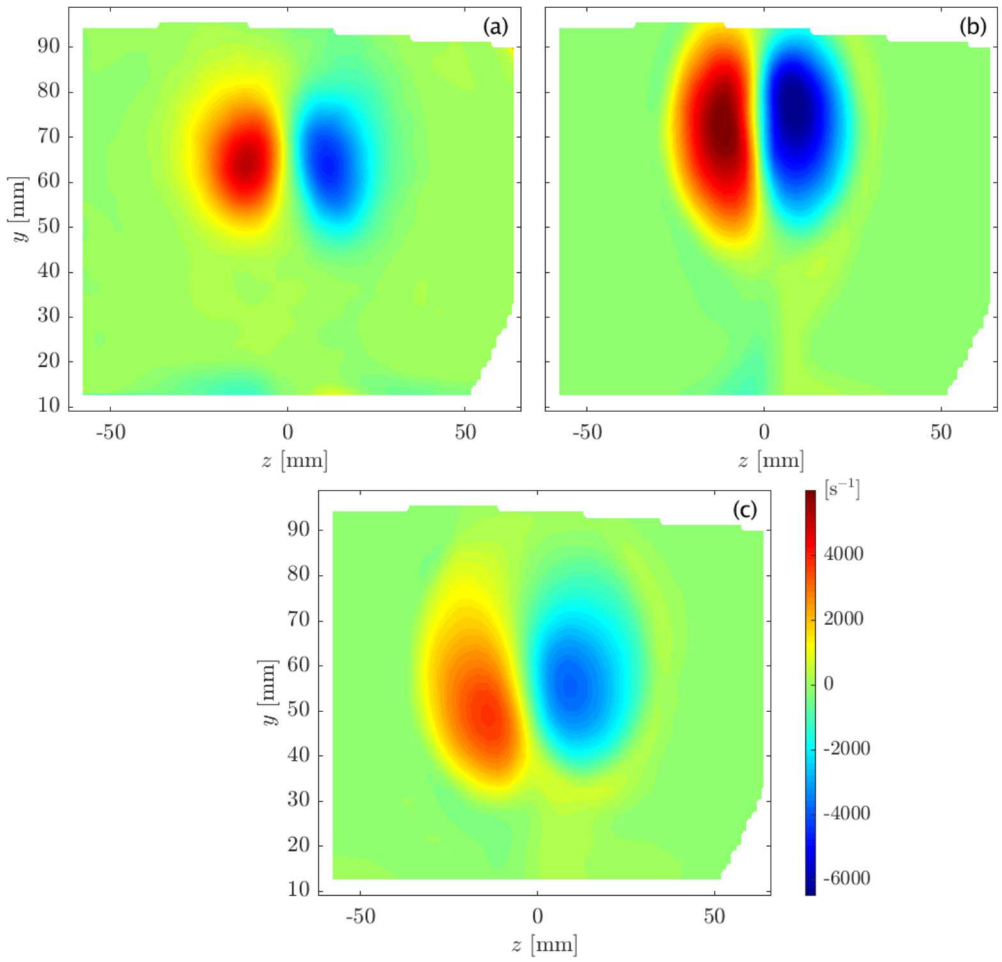

Figure 3: The streamwise vorticity on the crossplane at x = 219 mm for the α = 0° nozzle with J = 10.2 as collected from the PIV (a), as determined by RANS using the nominal parameter values (b), and using C_{opt} (c).

case when α = 30° and the data were taken at x = 219mm (Figure 4). These data were not used in determining C_{opt}, were taken from a somewhat more complicated flow, were taken at a different downstream location than were the data used for determining C_{opt}, and are more closely representative of a flight application of interest [8]. Both the locations of the vorticity cores and the magnitudes of the vorticity within those cores were improved with the use of C_{opt}. When the improvements seen by using C_{opt} were quantified using the quality metrics, all three reflected the qualitative observations by showing the C_{opt}-derived results to be a significant improvement over the C_{nom}-derived results (Table 4). The alignment of the inclined CVP was better, the magnitudes of the vorticity within the cores were better, and the mean errors were reduced throughout the crossplane.

One of the most rigorous tests of the calibrated k-ϵ parameters was when comparisons were made to the data taken in the vicinity of the full-scale flight vehicle. Given the cylindrical coordinate system of the vehicle and the clocking position of the jet nozzles on the vehicle body, velocities and gradients were defined based on the orientation of the vehicle in the wind tunnel and are therefore not specifically aligned with the nozzle exit normal as they were in the TWT. Direct

Table 3: Quality metrics for the streamwise vorticity on the crossplane as depicted in Figure 3.

	$corr$	MSE [1/s^2]	GME [1/s]
C_{nom}	0.841	0.756	1.05
C_{opt}	0.718	0.552	1.14

comparisons were then made for both V_y and $\overline{\omega}$ between the RANS and PIV data. Contours for $\overline{\omega}$ showed that the k-ϵ model with both sets of parameters was able to generate the correct general flow topology (Figure 5). Use of C_{nom} resulted in vortex cores with higher vorticity magnitudes and produced a second negatively oriented vortex core near the top of the PIV domain. The use of C_{opt} resulted in lower vorticity magnitudes than both the PIV and the C_{nom}-derived results, but also produced a better spatial alignment to the PIV data than did the use of C_{nom}. MSE, GME, and $corr$ were all improved for both V_y and $\overline{\omega}$ when C_{opt} was used (Table 5).

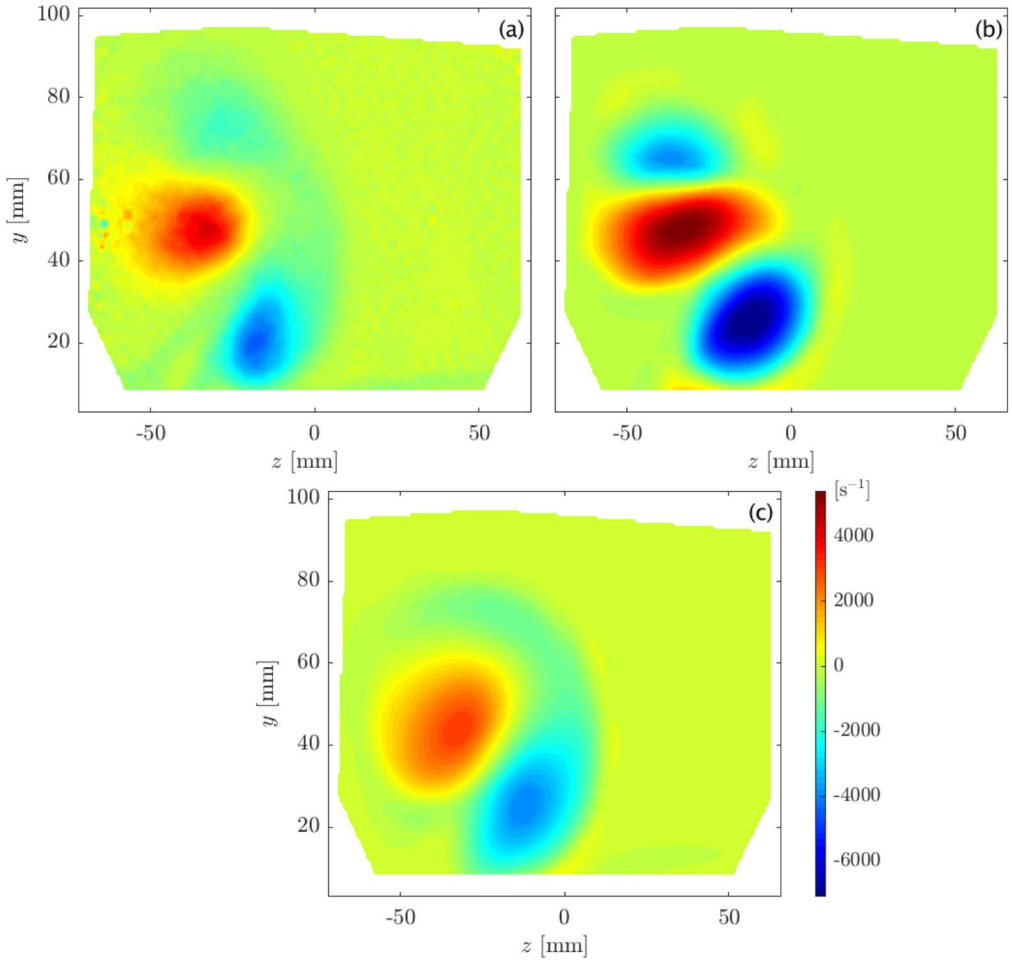

Figure 4: The streamwise vorticity on the crossplane at x = 219 mm for the α = 30° nozzle with J = 10.2 as collected from the PIV (a), as determined by RANS using C_{nom} (b), and using C_{opt} (c).

Table 4: Quality metrics for the streamwise vorticity on the crossplane as depicted in Figure 4.

	corr	MSE [1/s^2]	GME [1/s]
C_{nom}	0.853	0.987	1.00
C_{opt}	0.895	0.210	0.778

For the sake of brevity, no additional sets of contour plots are shown, but the three quality metrics were compared across all of the datasets for which the PIV could be compared to the RANS results. There were 24 planes of data on which comparisons were made between data taken in the TWT and the RANS results using each C_{nom} and C_{opt}. There was one additional plane on which comparisons were made to the PIV data taken in the vicinity of the full-scale flight vehicle tested in the tunnel at NASA Ames. V_y and $\overline{\omega}$ were again used, though the streamwise vorticity was not calculated on the x-y centerplanes. This resulted in 48 total comparisons between the data determined from the two different sets of RANS parameters and PIV data (Figure 6).

The MSE values determined when comparing the PIV data to the RANS results using C_{opt} were lower (better) than the MSEs determined based on C_{nom} in every one of the 48 comparisons (Figure 6(a)). This is a strong indication that the use of C_{opt} is a general improvement over using C_{nom} for these jet-in-crossflow experiments, regardless of the specific flow case. Using C_{opt} produced more accurate peak velocity and vorticity values than did C_{nom} in every case. It also appears that the improvement in MSE is somewhat more pronounced for the α = 0° and 15° cases than for the other inclination angles. This may be related to the fact that as α increases, the vortex cores stay closer to the wall and are increasingly tied to the boundary layer and HSV flow, thus reducing the complexity of the vortical structures being modeled [14]. The simpler flow fields of the cases with the higher nozzle inclination angles had less room for improvement than did the cases with the lower angles and were more similar to a wall-bounded flow, for which C_{nom} is known to perform relatively well. It may also be related to the fact that the α = 0° and 15° cases are the most similar to the case used for the calibration procedure that resulted in the determination of C_{opt}. The cases with the steeper inclination angles (and with the lowest Js) were the most different from the calibration case and therefore constitute a more extreme test of the applicability of C_{opt}. Regardless of the exact causes for the behavior of MSE versus α, the MSEs for all cases still showed improvements with C_{opt}.

When the GME results were investigated, a similar, though slightly less drastic result was found (Figure 6(b)). In 44 of the 48 comparisons, the RANS results based on C_{opt} produced a better GME measure than did the results based on C_{nom}. The four comparisons where the nominal approach remained slightly better than the calibrated approach were two comparisons of V_y on planes at x = 321.8 mm with α = 45° and J = 2.8 and 5.6, the comparison of the streamwise vorticity as discussed above (Table 3), and the comparison of V_y at x = 219 mm from that same α = 0°, J = 10.2 case. Contour plots of the mean velocities from the PIV for the cases with α = 45° and J = 2.8 and 5.6 can be found in Beresh *et al.* [14], and show the relative simplicity of the flow topology for those cases as discussed above. The use of C_{opt} reduced the peak velocity magnitudes correctly, resulting in the improved MSE values, but resulted in CVP cores that were more inclined than in the PIV or C_{nom} simulations. This inclination resulted in poor alignment of velocity values around the edges of the CVP cores, leading to slightly elevated GME values. These two cases were arguably the most different from the case used in determining C_{opt}. For the

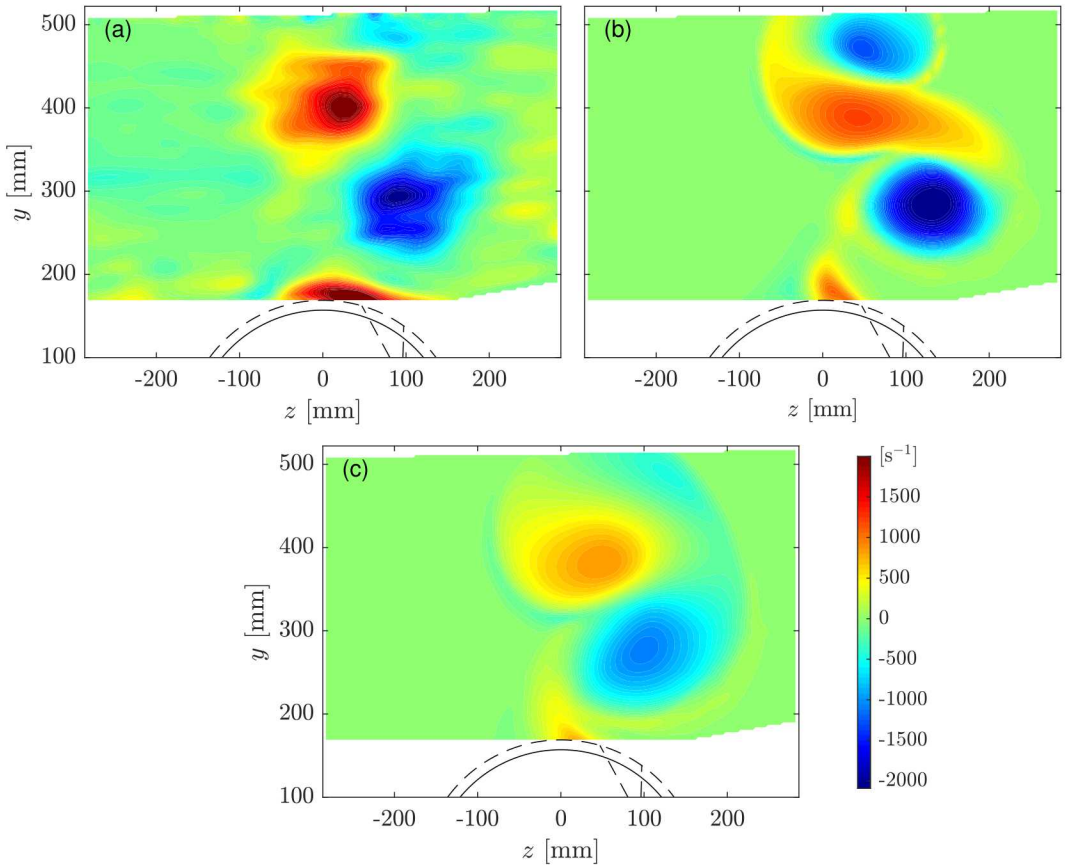

Figure 5: The streamwise vorticity on a y-z plane at x = 820 mm in the vicinity of the full-scale flight vehicle as viewed aft from the nose and as collected from the PIV (a), as determined by RANS using C_{nom} (b), and using C_{opt} (c). The dashed circles depict the diameter of the model at the axial location along the vehicle at which the nozzles were mounted, whereas the solid circle depicts the model diameter at the location at which the plane of PIV data was collected and is smaller due to the vehicle's boat-tailed design. The nozzle cross section and its approximate orientation are also depicted.

case with J = 5.6, this incorrect cant of the vortex cores also resulted in a poorer $corr$ value.

That poorer value was one of only six comparisons, from among the 48, where the correlation coefficient was slightly worse when C_{opt} was used instead of C_{nom} (Figure 6(c)). The remaining five comparisons where C_{nom} produced superior $corr$ values were the comparisons of vorticity taken from the same two α = 45° cases for which the GME of V_y was also worsened, the comparison of vorticity for the α = 0° case discussed above (Table 3), the comparison of V_y for that same α = 0°, J = 10.2 case, and the comparison of V_y on the centerplane as discussed above (Table 2). In each of these cases where either GME or $corr$ were not improved by the use of C_{opt}, the results were scarcely worse than when C_{nom} was used. The improvements to GME and $corr$ (and obviously MSE) for the remaining cases were typically much more drastic than were the declines in accuracy for the cases where they were worsened.

Table 5: Quality metrics for V_y and $\overline{\omega}$ on the plane collected in the vicinity of the full-scale flight vehicle as depicted in Figure 5.

		$corr$	MSE [1/s^2]	GME [1/s]
V_y:	C_{nom}	0.633	1.18	0.905
	C_{opt}	0.764	0.564	0.647
$\overline{\omega}$:	C_{nom}	0.651	0.649	0.974
	C_{opt}	0.843	0.363	0.796

V. Discussion, Conclusions, and Future Work

Taken as a whole, the use of C_{opt} does appear to produce superior RANS results than does using the nominal parameter values. Some of the results seen here could be partially conjectured from the later papers by Ray *et al*. In Ray *et al.* [21], the authors showed that high-order eddy viscosity models will not perform appreciably better than linear eddy viscosity models for the JIC dynamics, when both were tuned to data. This could indicate that perhaps that the linear eddy viscosity model was sufficient, provided that its parameters were appropriately calibrated. In Ray *et al.* [11], the authors tuned the same parameters to three other JIC interactions ((Mach 0.6, J = 10.2), (Mach 0.7, J = 10.2), and (Mach 0.8, J = 16.7)) and obtained estimates of $\{C_\mu, C_{\epsilon 1}, C_{\epsilon 2}\}$ that were similar to C_{opt}, indicating again that the calibrated C_{opt} would generalize beyond the (Mach 0.8, J = 10.2) case where C_{opt} was learned. The same paper derived analytical values for $\{C_\mu, C_{\epsilon 1}, C_{\epsilon 2}\}$ from first principles (i.e., without any data fitting or assuming that α = 0), leading one to conjecture that perhaps the calibrated values of $\{C_\mu, C_{\epsilon 1}, C_{\epsilon 2}\}$ represented physical processes inherent in JIC interactions rather than being artifacts of the fitting process. Consequently, there was some reason to believe that the tuned C_{opt} would be predictive for other, perhaps canted jet, interactions.

A weakness of the fitting performed in Ray *et al.* [10, 11] is the use of strong jets (J = 10.2, 16.7) that penetrated well into the crossflow and evolved with little interaction with the boundary layers on the wind-tunnel walls. This would indicate that the values of $\{C_\mu, C_{\epsilon 1}, C_{\epsilon 2}\}$ inferred in Ray *et al.* [10, 11] do not reflect turbulent processes involving CVP-to-boundary layer interactions, and C_{opt} would not be predictive in flows where the jet stays close to the wind-tunnel wall e.g., weak jets (J = 2.8, 5.6) and steeply canted jets (α = 45°). To a large extent, this paper bears out these conjectures. C_{opt} has been shown to be predictive in cases where the jet does not interact with the boundary layer. In the cases where it does (because of the cant or the weakness of the jet), C_{nom} remains better than C_{opt} according to some metrics. However, despite calibration, the linear eddy viscosity model has significant drawbacks. The move from C_{nom} to C_{opt} causes overshoots in the needed correction for some variables for some cases, but appears to do so as a trade-off for correcting magnitudes. Additionally, that overshoot in the correction may only be occurring in some portions of the domain while other portions are corrected by the right amount. This was seen in the data for the α = 0°, J = 10.2 case. The calibration procedure was performed on data from this case by Ray *et al.* [10] and indeed improved all six metric measurements (three metrics of two variables) at the x = 321.8 mm plane, but did so at the expense of the quality of the results at the x = 219 mm plane. This may point to larger limitations that exist with the structure of the RANS model itself.

One such limitation may be the use of constant scalar values for the model parameters. The potential variability of model parameters as a function of flow variables is not accounted for in most

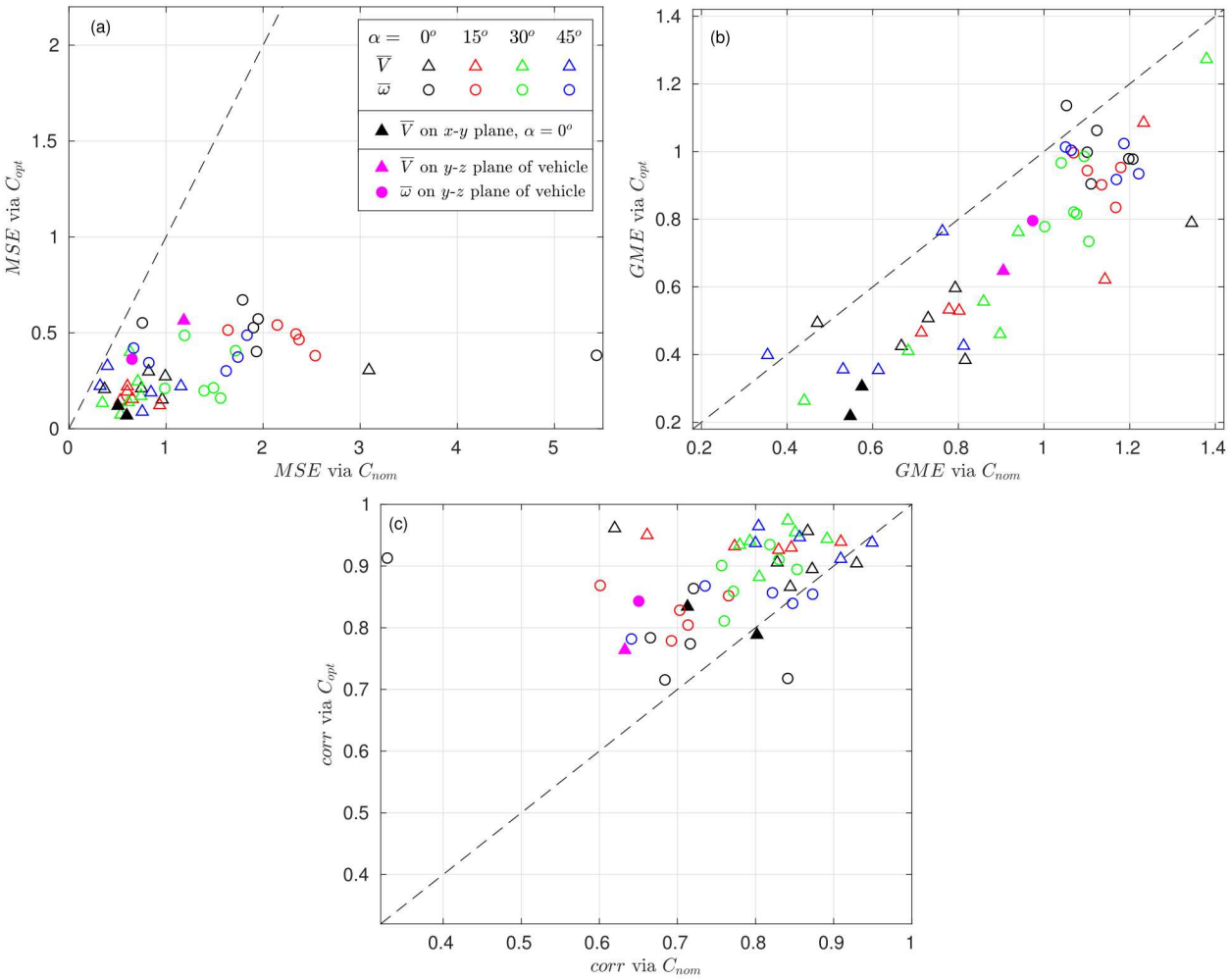

Figure 6: The three quality metrics as determined when comparing RANS results based on the use of C_{nom} and C_{opt} to the PIV data. The MSE (a), the GME (b), and the $corr$ (c) are compared. Open symbols indicate comparisons made on one of the two y-z planes of data from the TWT.

traditional RANS codes [22]. A new model, trained on experimental data, that can pick optimal values for the RANS parameters at every location in space, may be capable of producing better results. Philosophically, this approach would be very similar to the zone-dependent k-ϵ parameters demonstrated in Matai and Durbin [23]. The challenge in our case would be determining how to demarcate various zones and how to ensure logical, continuous values of $\{C_\mu, C_{\epsilon 1}, C_{\epsilon 2}\}$ within each zone. Development of such a model, using modern data science techniques, is ongoing, and early *a priori* testing of model training and testing has shown promising results. Final implementation may still prove to be unhelpful or unstable, or ideally, will prove to enhance model accuracy and robustness.

Acknowledgements

The authors wish to acknowledge Amalia Black and Jonathan Murray, both of Sandia National Laboratories, for their contributions to the production of the RANS data. This work was supported by multiple sub-programs under Sandia National Laboratories' Advanced Simulation and Comput-

ing (ASC) program. This paper describes objective technical results and analysis. Any subjective views or opinions that might be expressed in the paper do not necessarily represent the views of the U.S. Department of Energy or the United States Government.

References

[1] Beresh, S. J., Henfling, J. F., Erven, R. J., and Spillers, R. W., "Turbulent Characteristics of a Transverse Supersonic Jet in a Subsonic Compressible Crossflow," *AIAA Journal*, Vol. 43, No. 11, 2005, pp. 2385–2394.

[2] Kawai, S. and K., L. S., "Large-eddy Simulation of Jet Mixing in Supersonic Crossflows," *AIAA Journal*, Vol. 48, No. 9, 2010, pp. 2063–2083.

[3] Mahesh, K., "The Interaction of Jets with Crossflow," *Ann. Rev. Fluid Mech.*, Vol. 45, 2013, pp. 379–407.

[4] Karagozian, A. R., "The jet in crossflow," *Phys. of Fluids*, Vol. 26, 2014, 101303.

[5] Cassel, L. A., "Applying Jet Interaction Technology," *J. Spacecraft Rockets*, Vol. 40, 2003, pp. 523–537.

[6] Peterson, C. W., Wolfe, W. P., and Payne, J. L., "Experiments and computations of roll torque induced by vortex-fin interaction," *AIAA Paper 2004-1069*, January 2004.

[7] Beresh, S. J., Henfling, J. F., Spillers, R. W., and Pruett, B., "Influence of the Fluctuating Velocity Field on the Surface Pressures in a Jet/Fin Interaction," *J. Spacecraft Rockets*, Vol. 55, No. 5, 2018, pp. 1098–1110.

[8] Beresh, S. J., Heineck, J. T., Walker, S. M., Schairer, E. T., and Yaste, D. M., "Planar Velocimetry of Jet/Fin Interaction on a Full-Scale Flight Vehicle Configuration," *AIAA Journal*, Vol. 45, No. 8, 2007, pp. 1827–1840.

[9] Arunajatesan, S., "Evaluation of Two-Equation RANS Models for Simulation of Jet-in-Crossflow Problems," *AIAA Paper 2012-1199*, January 2012.

[10] Ray, J., Lefantzi, S., Arunajatesan, S., and Dechant, L., "Bayesian Parameter Estimation of a $k-\epsilon$ Model for Accurate Jet-in-Crossflow Simulations," *AIAA Journal*, Vol. 54, No. 8, 2016, pp. 2432–2448.

[11] Ray, J., Dechant, L., Lefantzi, S., Ling, J., and Arunajatesan, S., "Robust Bayesian Calibration of a $k-\epsilon$ Model for Compressible Jet-in-Crossflow Simulations," *AIAA Journal*, Vol. 56, No. 12, 2018, pp. 4893–4909.

[12] Beresh, S. J., Henfling, J. F., Erven, R. J., and Spillers, R. W., "Penetration of a Transverse Supersonic Jet into a Subsonic Compressible Crossflow," *AIAA Journal*, Vol. 43, No. 2, 2005, pp. 379–389.

[13] Beresh, S. J., Henfling, J. F., Erven, R. J., and Spillers, R. W., "Crossplane Velocimetry of a Transverse Supersonic Jet in a Transonic Crossflow," *AIAA Journal*, Vol. 44, No. 12, 2006, pp. 3051–3061.

[14] Beresh, S. J., Henfling, J. F., Erven, R. J., and Spillers, R. W., "Vortex Structure Produced by a Laterally Inclined Supersonic Jet in Transonic Crossflow," *J. of Prop. and Power*, Vol. 23, No. 2, 2007, pp. 353–363.

[15] Beresh, S. J., Wagner, J. L., Henfling, J. F., Spillers, R. W., and Pruett, B. O. M., "Turbulent Eddies in a Compressible Jet in Crossflow Measured using Pulse-Burst Particle Image Velocimetry," *Phys. of Fluids*, Vol. 28, No. 2, 2016, 025102.

[16] So, R. M. C., Sarkar, A., Gerodimos, G., and Zhang, J., "A Dissipation Rate Equation for Low-Reynolds-Number and Near-Wall Turbulence," *Theoret. Comput. Fluid Dynamics*, Vol. 9, 1997, pp. 47–63.

[17] Brinkman, K. W., Calhoon Jr., W. H., and Dash, S. M., "Scalar Fluctuation Modeling for High-Speed Aeropropulsive Flows," *AIAA Journal*, Vol. 45, No. 5, 2007, pp. 1036–1046.

[18] Chang, J. C. and Hanna, S. R., "Air quality model performance evaluation," *Meteorol Atmos Phys*, Vol. 87, 2004, pp. 167–196.

[19] Hanna, S. and Baja, E., "A simple urban dispersion model tested with tracer data from Oklahoma City and Manhattan," *Atmos. Environ.*, Vol. 43, 2009, pp. 778–786.

[20] Franzese, P. and Huq, P., "Urban Dispersion Modelling and Experiments in the Daytime and Nighttime Atmosphere," *Boundary-Layer Meteorol.*, Vol. 139, 2011, pp. 395–409.

[21] Ray, J., Lefantzi, S., Arunajatesan, S., and Dechant, L., "Learning an Eddy Viscosity Model Using Shrinkage and Bayesian Calibration: A Jet-in-Crossflow Case Study," *ASCE-ASME Journal of Risk and Uncertainty in Engineering Systems, Part B: Mechanical Engineering*, Vol. 4, No. 1, 2017, 011001.

[22] Miller, N. E., Beresh, S. J., and Barone, M., "Direct Calculation of RANS Model Parameters from Jet-in-Crossflow PIV Data," *AIAA Paper 2019-1872*, January 2019.

[23] Matai, R. and Durbin, P. A., "Zonal Eddy Viscosity Models Based on Machine Learning," *Flow Turbul. Combust.*, 2019, https://doi.org/10.1007/s1049.